A universal scaling for the length scales of shock-induced separation

Sébastien Piponniau, Pierre Dupont, Nikhil Mahalingesh

A universal scaling for the length scales of shock-induced separation

Nikhil Mahalingesh[1], Sébastien Piponniau[1] †, and Pierre Dupont[1]

[1]Aix Marseille Univ, CNRS, IUSTI, Marseille, France

(Received xx; revised xx; accepted xx)

Experiments of transitional shock wave boundary layer interactions over a 6° and a 10° compression ramp were performed at a Mach number of 1.65. The unit Reynolds number was varied by a factor of two between 5.6 million per metre and 11 million per metre. Schlieren flow visualization was performed, and mean flow measurement were made using Pitot probes. Free-interaction theory was verified from pressure measurements for all operating conditions. A new non-dimensional parameter was developed for scaling the strength of the imposed shock, that incorporated free-interaction theory, and accounted for Reynolds number effects. The validity of this new scaling was supported by the reconciliation of the large scatter in a diverse collection of experimental results on the length scales of transitional interactions. Finally, a universal scaling for the length scales of shock induced separation with laminar or turbulent upstream conditions is proposed.

Key words:

1. Introduction

Shock wave boundary layer interaction (SBLI) is a classical flow phenomenon of high speed aerodynamics. SBLIs are encountered in various applications such as engine inlets, transonic wings, rocket nozzles, compressors, etc. and hence, has received a lot of attention over the past 70 years (Délery *et al.* 1986; Dolling 2001).

While small imposed flow deflections tended only to thicken the boundary layer, stronger flow deflections resulted in boundary layer separation. It was understood that one of the important mechanisms of SBLIs was the upstream propagation of the incident pressure rise through the subsonic channel of the boundary layer (Lees 1949). Given how often SBLIs were encountered in practical applications, there began many investigations with the objective to develop a model to predict the length of the separated region.

However, this length scale was depended on many parameters such as Mach number, Reynolds number, imposed flow deflection, and more importantly, on the type of upstream boundary layer. In fact, SBLIs can be classified into three types, depending on the location of boundary layer transition (Gadd *et al.* 1954):

† Email address for correspondence: sebastien.piponniau@univ-amu.fr

(i) Laminar interactions: where the boundary layer remained laminar throughout the interaction.

(ii) Transitional interactions: where the boundary layer was laminar before separation and became turbulent after reattachment.

(iii) Turbulent interactions: where the boundary layer was "fully" turbulent before the interaction.

The length of interaction (L) (formally defined as the stream-wise distance between the imposed (inviscid) shock location at the wall and mean location of boundary layer separation at the wall) for laminar interactions were much larger compared to turbulent interactions. Even when scaled with their respective boundary layer thicknesses, the measurements highlighted that $L/\delta^* \approx \mathcal{O}(10^1)$ for turbulent and $L/\delta^* \approx \mathcal{O}(10^2)$ for laminar interactions, for equivalent Mach, Reynolds numbers and flow deflections.

Additionally, the flow deflection (or equivalently the pressure rise) required to separate a laminar boundary layer was much lower when compared to turbulent boundary layers (Liepmann *et al.* 1952). This meant that it was difficult to make a fair comparison between the different types of SBLIs.

When comparing the same type of SBLIs, free-interaction theory (first proposed by Oswatitsch & Wieghardt (1948) and later formalized by Chapman *et al.* (1958)), showed that the non-dimensional pressure rise at separation was independent of the imposed flow deflection, but rather only a function of the upstream Mach and Reynolds number. This meant that the coefficient of free-interaction was different depending on the type of upstream boundary layer (Babinsky & Harvey 2011).

Further, the length of interaction was found to be dependent on the type of geometrical configuration; while a small compilation of oblique shock reflection experiments did show the same linear relationship between the length scales and the imposed shock strength (Dupont *et al.* 2006), the length scales from compression ramp experiments were approximately 2 to 4 times smaller for equivalent shock strengths.

The pioneering work of Souverein *et al.* (2013) was able to develop scaling laws for both the length of interaction as well as the shock strength, to collapse the majority of the experimental measurements of turbulent SBLIs. It was shown that the length of interaction was the direct consequence of the mass flow deficit between the outgoing and incoming boundary layer. This scaling was a common formulation for both oblique shock reflections as well as compression ramps.

Moreover, it was shown that the pressure needed to separate a turbulent boundary layer was mainly dependent on the dynamic pressure of the freestream, and only a weak effect of Reynolds number was reported (see figure 7, pg. 519, Souverein *et al.* (2013)). Hence, an inviscid shock strength was developed which was a type of overall pressure difference across the interaction, expressed in non-dimensional form.

The compilation of a number of experimental measurements of turbulent SBLI using this scaling can be seen in figure 1. This scaling was successfully able to clear the ambiguities associated with the length scales of turbulent SBLIs between various wind tunnel facilities over a large range of Mach numbers, Reynolds numbers, and flow deflections.

However, Reynolds number was found to have a significant effect on transitional interactions. Large differences (approximately 50%) were reported between the length scales from low Reynolds number wind tunnel of the IUSTI laboratory (Diop *et al.* 2016, 2019) and the high Reynolds number wind tunnel of TU Delft (Giepman *et al.* 2018), for the same imposed shock strength.

A possible explanation was also the difference in free-stream noise of the two wind tunnels, which could have affected the transition process of the separated laminar boundary layer, and indirectly affected the length scales of the interaction. The wind tunnel of the IUSTI

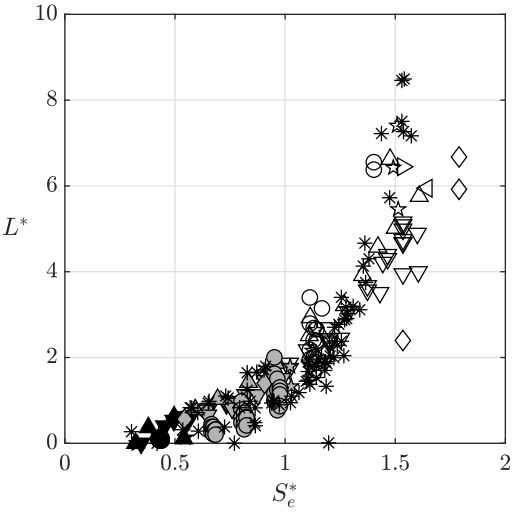

Figure 1: Collapse of turbulent SBLI experiments using the mass-balance scaling (legend: refer to Souverein *et al.* (2013)).

laboratory was found to have approximately 4 times lower turbulent intensities (in terms of mass-flux fluctuations). On a similar note, numerical studies of oblique shock reflections showed that the amplitude of inflow perturbations had a significant influence on the length of interaction (Larchevêque 2016), similar to what was observed for low speed laminar separation bubbles (Marxen & Henningson 2011). Hence, transition of the laminar boundary layer also played a significant role in affecting the length scales in such types of interactions.

Hence, it was clear that the length scales of transitional SBLIs were sensitive to more parameters compared to turbulent SBLIs. Consequently, a thorough search of literature did not yield any scaling laws or comprehensive compilation for laminar and transitional SBLIs, that accounted for the effects of Reynolds number.

The main aim of the current paper is to investigate the length scales of transitional SBLI with the hope of reconciling the discrepancies between different wind tunnel facilities. It is well known that length scales of such interactions have a complicated relationship with the transition of the boundary layer. The effect of Reynolds number and receptivity of the boundary layer to free-stream disturbances, is not very well understood. As several experimental facilities have examined the length scales of laminar and transitional SBLIs, the current work explores whether a scaling can be developed that consolidates all these results. Lastly, an effort is made to develop a common model for laminar, transitional and turbulent SBLIs.

Experiments studying transitional SBLIs were performed with two compression ramps and comparisons were drawn with previous experiments from the IUSTI laboratory. The paper is organized as follows. Section 2 describes the experimental facilities of the IUSTI laboratory along with the geometrical models and the flow measurement techniques that were used. Sections 3.1 and 3.2 verifies and validates the canonical nature of the upstream laminar boundary layer as well as the compression ramp SBLIs respectively. The length of interaction is addressed in section 3.3, initially focusing on the effect of flow deflection and Reynolds number, and then moving on to the compilation of experimental data. Section 3.4 extends the scaling to turbulent SBLIs and comparisons are drawn between different types of interactions. Section 4 summarises the results, providing conclusions and perspectives.

2. Experimental Methodology

The experiments were performed at the IUSTI laboratory of Aix-Marseille University and CNRS. The supersonic wind tunnel was a closed-loop system which could be continuously operated for several hours without significant drift in free-stream properties (±1K/hr and ±0.5 mbar).

Experiments were performed in the S8 test section, where a symmetric converging-diverging nozzle accelerated the flow to a Mach number of 1.65, corresponding to a free-stream velocity of 464 m/s. The total temperature was maintained at ambient conditions (approximately 295 K, depending on weather conditions), while the total pressure (p_t) of the free-stream could be varied from 0.15 atm (near vacuum) to 0.9 atm (close to ambient pressure). This resulted in a range of unit Reynolds numbers (Re_u) from $2.1 \times 10^6\ m^{-1}$ to $12.4 \times 10^6\ m^{-1}$ for the free-stream. Most of the current experiments were performed for freestream total pressures of 0.4 atm, 0.6 atm and 0.8 atm (table 1).

The free-stream noise at the exit of the nozzle was measured using the classical single sensor hot-wire anemometer. The Streamline amplifier from Dantec Dynamics was operated in the symmetric bridge configuration. A platinum and tungsten wire of 2.5µm diameter was used. The constant temperature anemometer had an effective bandwidth in the range of 100 kHz to 150 kHz, depending on the unit Reynolds number. Table 1 shows the measured turbulence intensities in terms of non-dimensional fluctuations (root mean square) of mass-flux, velocity and pressure. The free-stream noise was found to be hypo-turbulent in nature, with low turbulence intensities for all operating conditions. Thus, ensuring that the laminar boundary layer would not undergo bypass transition (Laufer 1961).

Downstream of the nozzle, the test section was 105 mm in height and 170 mm in span-wise width. The geometric models of the two compression ramps were similar in construction with a sharp leading edge, total length of 280 mm and spanning the entire width of the test section. The location of the corner of the ramp (x_c) was 115 mm from the leading edge for both ramps. Reynolds number based on the location of the corner is shown in table 1 for different total pressures of the free-stream. The two models were placed at a height of 25 mm from the floor, using supports near the span-wise edges of the wind tunnel. Pictures and schematics of the two models are shown in figures 2 and 3. It is to be noted here that the adiabatic wall temperature for these models nearly reached ambient conditions (total temperature of the freestream), considering a recovery factor: $r \approx Pr^{1/2} \approx 0.84$ for a fully laminar boundary layer and $r \approx Pr^{1/3} \approx 0.89$ for a fully turbulent boundary layer (Mack 1954), where Pr is the Prandtl number.

The flow deflection (φ) of the two compression ramps were chosen such that direct comparisons could be drawn with the oblique shock reflection experiments by Diop (2017). In particular, the ramp angles were chosen to be twice that of the imposed flow deflection in the oblique shock reflection experiments, so that the overall pressure rise across the interaction were the same between the two configurations (Délery *et al.* 1986). The oblique shock reflection experiments were performed in the same wind tunnel facility (but in the other test section (S7) of the IUSTI laboratory), at similar Mach and Reynolds numbers. Similar to experiments of Diop (2017), the floor of the wind tunnel was modified to have an additional depth of 10 mm to alleviate choking of the secondary flow underneath the models.

Flow visualization was performed using Schlieren measurements from a conical setup involving a parabolic mirror. Vertical gradients of density in the flow were visualized by placing the knife edge horizontally. Images were acquired at low speeds with a classical full-frame digital SLR camera (Nikon D700), having a 12-bit CMOS sensor with a pixel size of 8.45 μm, and a resolution of 4526 × 2832 pixels, and the exposure time of the camera was set to 150 μs.

p_t [atm]	M	Re_u ($\times 10^6$) [m^{-1}]	Re_c ($\times 10^6$)	$\sigma_{\rho u}$ [%]	σ_u [%]	σ_p [%]
0.4	1.64	5.61	0.65	0.07	0.04	0.16
0.6	1.64	8.37	0.96	0.06	0.03	0.13
0.8	1.65	11.01	1.27	0.05	0.03	0.11

Table 1: Operating conditions of the experiments.

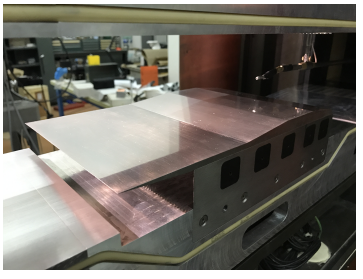

(a) Picture.

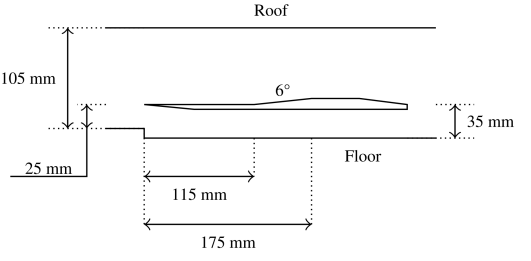

(b) Schematic.

Figure 2: 6° compression ramp geometrical configuration.

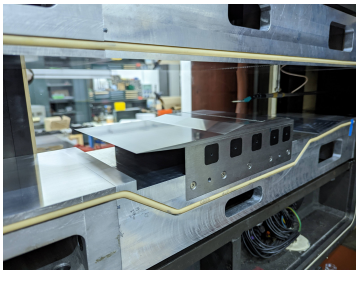

(a) Picture.

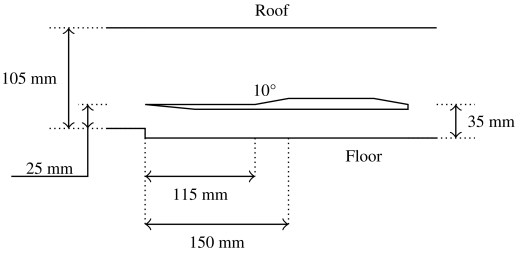

(b) Schematic.

Figure 3: 10° compression ramp geometrical configuration.

A classical Pitot probe was used to make measurements of the mean flow field. The tip of the probe was 0.3 mm in height with a opening of 0.15 mm in height, which measured the mean stagnation pressure of the flow. Flow properties such as Mach number, pressure, temperature, velocity and density were determined using standard equations.

3. Results

3.1. *Upstream boundary layer*

The boundary layer velocity profiles were measured at different stream-wise locations on a simple flat plate geometry at the same Mach number. The geometry and setup of the flat plate was identical to both the compression ramps.

Measurements using the Pitot probe were made every 0.05 mm in the wall-normal coordinate and are shown in figure 4 in similarity coordinates, with stream-wise velocity scaled with the external velocity outside the boundary layer (u_e) and wall-normal distance

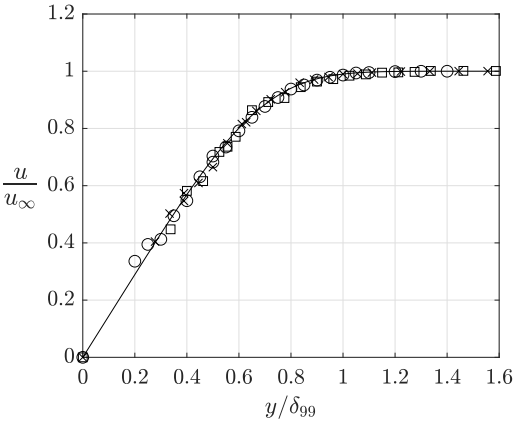

Figure 4: Boundary layer velocity profiles at different Reynolds numbers. Legend: solid black line: Blasius boundary layer;
$\circ$ $Re_x = 0.65 \times 10^6$; $\times$ $Re_x = 0.96 \times 10^6$; $\square$ $Re_x = 1.27 \times 10^6$.

scaled with the boundary layer thickness (δ_{99}). The figure also shows the theoretical compressible Blasius boundary layer profile, obtained by solving the compressible boundary layer equations for the same Mach number.

Measurements of the boundary layer profile made at different Reynolds numbers exhibited a clear linear region and agreed very well with the theoretical Blasius profiles. Thus, validating the canonical nature of the laminar boundary layer for the Reynolds numbers (i.e. Re_c) considered in the current experiments (table 1). The nature of the boundary layer was expected to be the same over both compression ramps, given the similarity of the geometrical models. Hence, it was concluded that both compression ramps were interacting with a canonical laminar boundary layer.

3.2. *Spatial organization*

Figure 5 shows the Schlieren visualization of the transitional SBLI for the 6° compression ramp. The sensitivity of the Schlieren system was increased so that small density gradients may be observed more clearly. A weak shock wave from the leading edge of the ramp (annotated by LE Shock) was seen. A weak Mach wave was seen originating from the ceiling of the test section, upstream of the leading edge. This Mach wave was due to a microscopic structural discontinuity between the end of the diverging section of the nozzle and the start of the test section. Due to the weak strength of this Mach wave, no significant effect was observed on the mean flow field of the interaction, based on Pitot probe and hot-wire measurements. Additionally, the secondary flow (under the ramps) appeared to maintain supersonic conditions, indicating that the flow was not choked.

Looking closely near the corner, it was seen that the boundary layer separated upstream of the corner and subsequently re-attached downstream of the corner. A separation bubble was visible between the points of separation and reattachment (identified by the small bright white region). Separation of the boundary layer was not characterized by a distinct shock wave, but rather weak compression waves which could not be seen by Schlieren imaging. However, stronger compression waves were observed at reattachment, which coalesced further away from the wall and merged in to a shock wave. The Schlieren visualization of the interaction involving the 10° compression ramp was similar and is not shown here to avoid repetition.

An illustration of the compression ramp SBLI is shown in figure 6, where C represented the corner of the ramp, with S and R representing separation and reattachment of the boundary

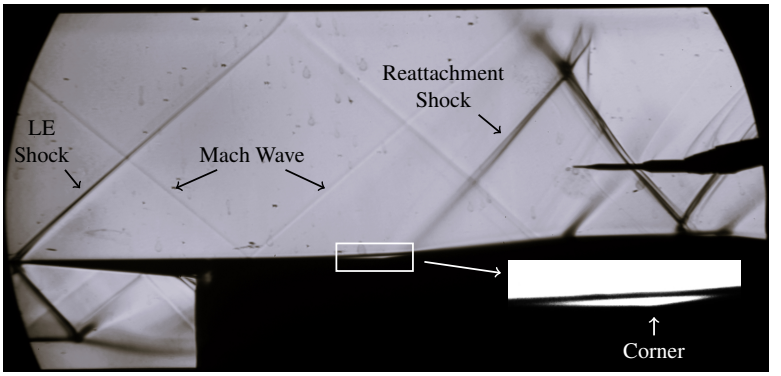

Figure 5: Schlieren visualization for $\varphi = 6°$ & $Re_c = 0.65 \times 10^6$.

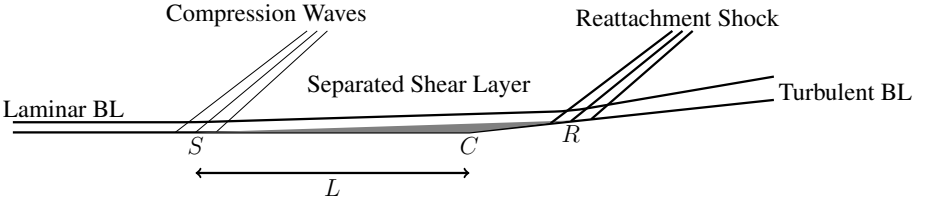

Figure 6: Illustration of the SBLI over the compression ramp.

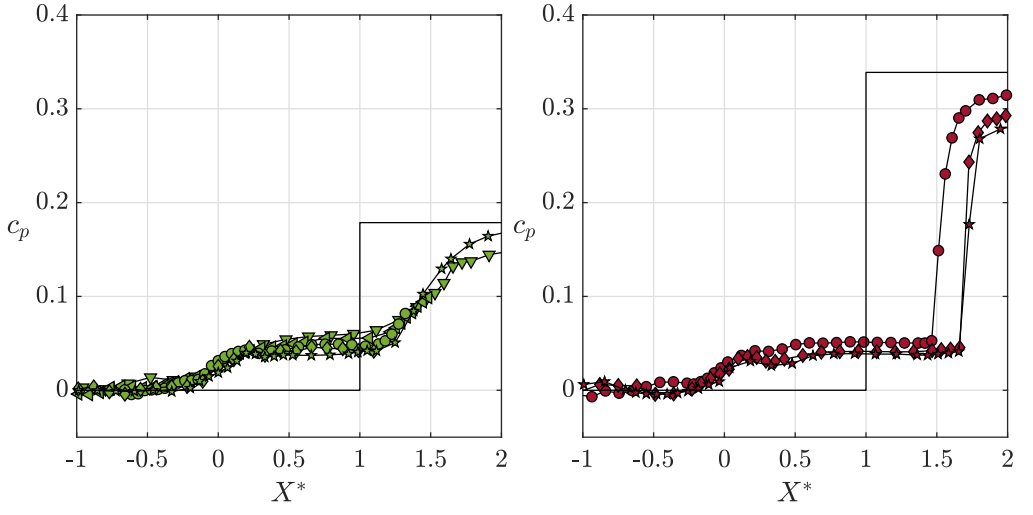

(a) 6° ramp. (b) 10° ramp.

Figure 7: Comparison of Pitot pressure evolution with inviscid pressure rise (legend: refer to table 3, solid black line represents the inviscid pressure step).

layer respectively. The recirculating region was long and thin, shown by the gray region between the points S and R. Such large aspect ratios of the separated region was also found by previous studies (Diop *et al.* 2019; Giepman *et al.* 2018; Threadgill *et al.* 2021). Far downstream of reattachment, the boundary layer was expected to be fully turbulent. The stream-wise distance between the points S and C was referred to as the length of interaction (L).

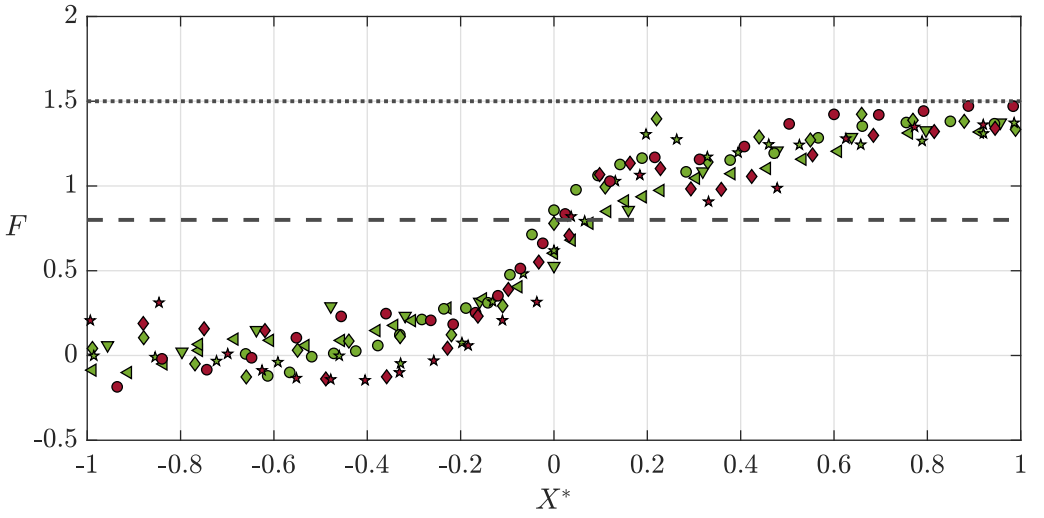

Figure 8: Pressure evolution across separation represented through the coefficient of free-interaction (legend: refer to table 3, dashed black line corresponds to $F_s = 0.8$, and dotted black line corresponds to $F_p = 1.5$).

Figure 7 shows the evolution of the static pressure coefficient over the interaction for the two compression ramps, measured using the Pitot probe. Measurements were made outside the boundary layer at a constant height from the wall, for every 1 mm along the stream-wise coordinate. The height of the measurements was chosen such that there was minimal probe interaction effect on the flow. This was chosen to be $y = 5$ mm and $y = 14$ mm for the 6° and 10° compression ramps respectively.

The stream-wise coordinate was normalized according to equation 3.1, where x_s corresponded to the mean location of separation and x_c was the location of the corner.

$$X^* = \frac{x - x_s}{x_c - x_s} \tag{3.1}$$

The mean location of separation was associated with the inflection point in the stream-wise pressure evolution. This inflection point was determined by identifying the peak in the stream-wise gradient of the pressure. Thus, the mean location of separation was determined up to an accuracy of ±1 mm.

The measurements showed a classical two-step pressure rise, characteristic of separated SBLIs, for all the operating conditions of the current experiments. Comparisons were also made with the inviscid pressure rise for each compression ramp, and reasonable agreement was found in both cases, with a small undershoot by the experiments. This was due to the non-trivial loss of total pressure across the reattachment shock, which was not taken into account in the data analyses. The reattachment pressure rise was more spread out on the 6° ramp compared to the 10° ramp, suggesting that the reattachment compression was more smooth for the 6° ramp.

The non-dimensional pressure rise at separation was identical for both compression ramps, owing to the free-interaction process of the boundary layer (Chapman *et al.* 1958). Figure 8 shows the evolution of the pressure across separation in terms of the coefficient of free-interaction (F):

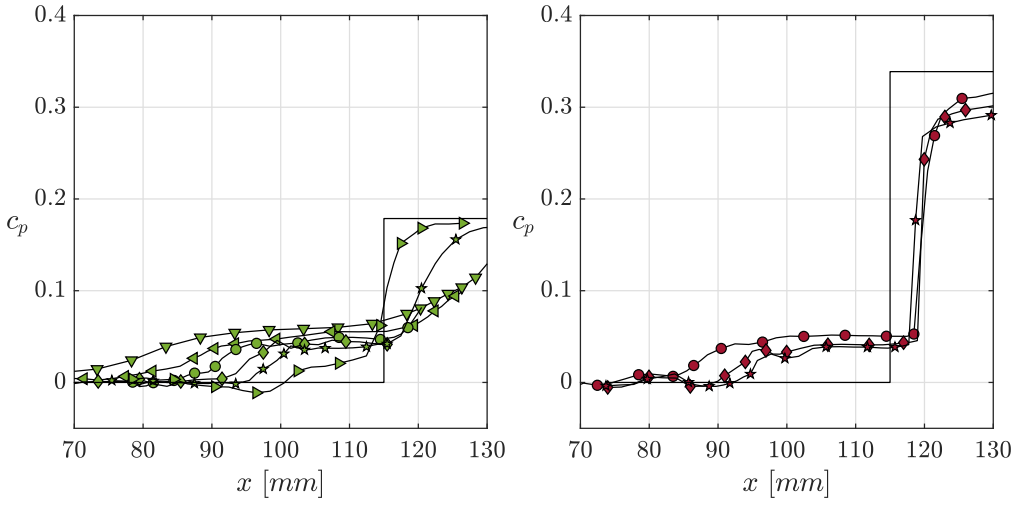

(a) 6° ramp. (b) 10° ramp.

Figure 9: Comparison of non-dimensional pressure evolution (legend: refer to table 3, vertical solid black line corresponds to location of the corner).

$$F = \frac{p - p_1}{q}\sqrt{\frac{(M^2-1)^{1/2}}{2\,c_f}} \tag{3.2}$$

Where p_1 was the static pressure of the freestream, q was the dynamic pressure of the freestream, and c_f was the skin-friction coefficient. The theoretical skin-friction coefficient from an equivalent (attached) Blasius boundary layer was used to determine this coefficient. It is to be noted here the theory of free-interaction proposed another scaling for the stream-wise coordinate based on the extent of the pressure rise at separation. This scaling was not used here as it was not possible to accurately and confidently determine this stream-wise length. Hence, figure 8 uses the scaling based on the length of interaction (equation 3.1). Nevertheless, the measurements confirmed the process of free-interaction, as a value of $F_s \approx 0.8$ was reached at the mean location of separation and the pressure asymptotically reached $F_p \approx 1.5$ downstream of separation, agreeing with standard values reported by various experiments in literature (Babinsky & Harvey 2011). This confirmed the canonical nature of the current compression ramp SBLIs.

The flow deflection at separation (corresponding to the pressure rise at separation) was found to be $1.3° \leq \varphi_s \leq 1.7°$. It was observed that this flow deflection at separation decreased slightly with increasing Reynolds number, following the predictions of free-interaction theory (Chapman *et al.* 1958). However, the exact difference in these flow deflections were within the uncertainty of the measurements, and hence, this result could not be concluded with confidence. Nevertheless, the global organization of the mean flow field was similar for the two compression ramps for all the Reynolds numbers considered in these experiments.

3.3. *Length of interaction*

Additionally, Pitot probe measurements provided quantitative insight into the upstream influence of the SBLI through the length of interaction, which was defined as the stream-wise distance between the corner of the ramp and the mean location of boundary layer separation (measured at the wall). Figure 7 showed that the global organization of the mean flow was

		φ	
		6°	10°
Re_c ($\times 10^6$)	0.24	34.8	
	0.33	27.2	
	0.65	22.1	26.0
	0.96	19.2	20.7
	1.27	16.2	19.0
	1.43	14.3	

Table 2: Absolute lengths of interactions shown in millimetres.

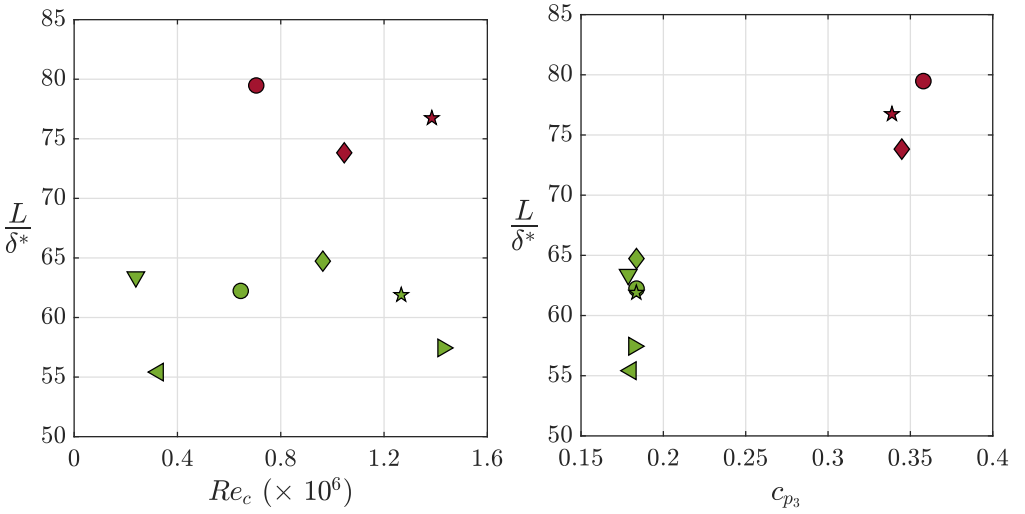

(a) Reynolds number effect.

(b) Shock strength effect.

Figure 10: Comparison of non-dimensional lengths of interaction between both compression ramps (legend: refer to table 3).

similar for both ramp geometries. However, it did not show how the length of interaction changed with Reynolds number as well as imposed flow deflection. Figure 9 compares the pressure evolution over the interaction between the two ramps, similar to figure 7 (Here, data is shown for more Reynolds numbers on the 6° compression ramp to highlight the effect of Reynolds number). But instead of using the non-dimensional stream-wise coordinate, the stream-wise coordinate was projected to the wall (using the local Mach characteristic angles), and is shown in absolute units of millimetres.

It was observed that the length of interaction decreased when Reynolds number was increased, for both the ramps. And comparing between the two ramps, the length of interaction was larger for higher ramp angles (table 2). Additionally, it was observed that on the 6° ramp, both the location of separation (corresponding to the first pressure rise) and reattachment (corresponding to the second pressure rise) moved when the Reynolds number was changed. However, only the location of separation moved and the reattachment point was nearly fixed at approximately the same location on the 10° ramp.

Figure 10 highlights the evolution of the length of interaction (L) normalized by the compressible displacement thickness (δ^*) at separation (the theoretical compressible displacement thickness for an attached Blasius boundary layer was used). The same symbols used in figure 9 were repeated for consistency. Here, the shock strength was defined as the non-dimensional inviscid pressure rise imposed by the ramp:

$$c_{p_3} = \frac{p_3 - p_1}{q} = \frac{2}{\gamma M^2}\left(\frac{p_3}{p_1} - 1\right) \tag{3.3}$$

Where p_3 was the "final" pressure downstream of the reattachment. A clear trend of the length of interaction was not observed for increasing Reynolds numbers (figure 10a). Moreover, the length scales for different Reynolds numbers fell on a vertical line for each ramp (figure 10b). Hence, it was important to incorporate Reynolds number in the non-dimensional scaling of the shock strength.

Further, for comparisons to be made between different geometries (e.g. oblique shock reflections and compression ramps), there was a need to utilise a common length scaling for both geometries. As the current experiments were made so that a direct comparison could be made with oblique shock reflection experiments of Diop (2017), an effective scaling for the length of interaction was necessary. Souverein *et al.* (2013) developed a common length scaling for turbulent SBLIs, based on the mass flow deficit between the outgoing (m_{out}) and incoming (m_{in}) boundary layer.

$$L^* = \frac{L}{\delta^*}G_3 = \frac{L}{\delta^*}\left(\frac{\sin(\beta)\sin(\varphi)}{\sin(\beta-\varphi)}\right) = \left(\frac{m_{out}}{m_{in}} - 1\right) \tag{3.4}$$

Where δ^* was the compressible displacement thickness of the boundary layer at the mean location of separation, β was the inviscid shock wave angle, and φ was the imposed flow deflection. This scaling was a common formulation for both oblique shock reflections as well as compression ramps. Although this scaling was developed for turbulent SBLIs, it should also be applicable to transitional SBLIs, given that this formulation was developed on a mass conservation basis.

Figure 11 compares the length of interaction between the current experiments on compression ramps and oblique shock reflection experiments from Diop (2017). The legend of the symbols used in this figure can be found in table 3. Here, Re_i refers to the Reynolds number based on the location of the inviscid shock at the wall (impingement shock for the oblique shock reflection and location of the corner for compression ramps). This common notation of Reynolds number will be used from here onwards to avoid confusion.

It was observed that the classical normalization (L/δ^*) resulted in nearly half the interaction lengths for the compression ramps compared to the oblique shock reflections (figure 11a). The use of "mass-balance" length scaling (L^*) rectified this disagreement. Further, length scales for equivalent shock strengths nearly collapsed on each other and the same linear relationship was obtained between the non-dimensional shock strength and the non-dimensional length of interaction (figure 11b). This confirmed that such a length scaling based on the mass-balance approach was also valid for transitional SBLIs.

Additionally, Souverein *et al.* (2013) also proposed a non-dimensional separation criterion to classify the shock strength:

$$S_e^* = \frac{p_3 - p_1}{(\Delta p)_{sep}} = k\frac{2}{\gamma M^2}\left(\frac{p_3}{p_1} - 1\right) \tag{3.5}$$

Here, a constant (k) was chosen such that it took into account the weak effect of Reynolds

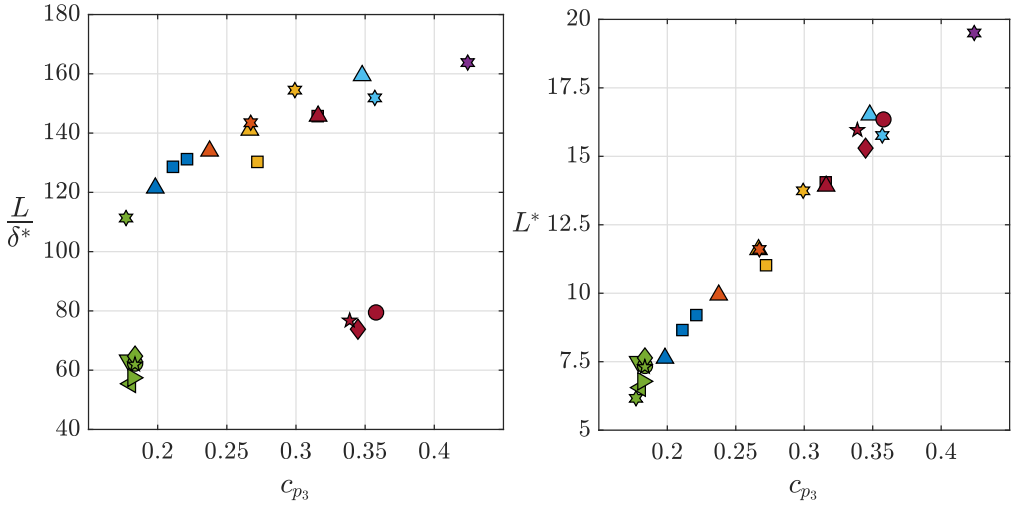

(a) Classical normalization. (b) Mass-balance normalization.

Figure 11: Comparison of lengths of interaction between compression ramps and oblique shock reflections (legend: table 3).

Oblique shock reflections (Diop 2017)

Re_i ($\times 10^6$)	φ 3°	3.5°	4°	4.5°	5°	5.5°	6°
0.62		■		■	■		
0.92		▲	▲	▲	▲	▲	
1.24	★		★	★		★	★

Compression ramps (current experiments)

Re_i ($\times 10^6$)	φ 6°	10°
0.24	▼	
0.33	◀	
0.65	●	●
0.96	♦	♦
1.27	★	★
1.43	▶	

Table 3: Legend of symbols for transitional SBLI experiments of the IUSTI laboratory.

number as well as expressed the separation state of the boundary layer. Particularly, the constant was chosen as $k = 3$ for $Re_\theta \leq 10^4$ and $k = 2.5$ for $Re_\theta > 10^4$ so that $S_e^* = 1$ at the onset of separation, with $S_e^* < 1$ corresponding to incipiently separated interactions and $S_e^* > 1$ corresponding to fully separated interactions.

This was similar to the shock strength scaling used here (comparing equations 3.3 and 3.5), but with an additional parameter (k). It was shown that the Reynolds number did not have a significant effect in turbulent SBLIs, or more specifically, the "pressure difference" required to separate a turbulent boundary layer $\left((\Delta p)_{sep}\right)$ had a weak dependence on Reynolds number.

The use of such a separation criterion for transitional SBLIs meant that this constant had to be modified from what was typically used for turbulent SBLIs. Particularly, the value of this constant had to be increased, as the pressure difference required to separate a laminar boundary layer $\left((\Delta p)_{sep}\right)$ was much smaller compared to turbulent boundary layers. Moreover, the values of L^* in transitional SBLIs were much larger compared to turbulent SBLIs (comparing figures 1 and 11). Extrapolating the values of L^* found by Souverein *et al.* (2013) to the values reported in figure 11, a value of $k \approx 9$ was chosen for transitional SBLIs. It is important to note that the value of this constant will only introduce an offset to the horizontal axis for the data points on figure 11.

As the set of data in figure 11 was quite limited (similar Mach numbers, Reynolds numbers, and flow deflections), it was difficult to determine whether a new scaling worked better than the classical one. Hence, an attempt was made to compile a number of experimental measurements of the lengths of interaction for transitional SBLIs. Particularly, experiments of oblique shock reflections and compression ramps were collected. The current data set was limited to the supersonic regime and excluded hypersonic experiments. It was believed that the non-adiabatic wall conditions in hypersonic experiments might locally influence the pressure required to separate the boundary layer. Due to the complexity of this effect, hypersonic experiments were excluded in the current compilation. Figure 12 shows the compilation of the experiments using the scaling proposed by Souverein *et al.* (2013). The legend for this compilation is shown in table 4.

This compilation was not exhaustive and did not include the length scales reported from the following transitional SBLI experiments, as the published information was not enough to determine L^* and S_e^*: Liepmann *et al.* (1952), Gadd *et al.* (1954), Gadd (1958), Lewis *et al.* (1968), Roberts (1970), and Polivanov *et al.* (2015).

Nevertheless, this compilation had a collection of independent experiments performed over the past 70 years, in different wind tunnel facilities, and with a wide range of operating conditions:

$$1.6 \leq M \leq 4.0$$

$$0.11 \leq Re_i \ (\times 10^6) \leq 2.5$$

$$1.2 \leq p_3/p_1 \leq 8.3$$

It is important to note that such a compilation was made for the first time for laminar and transitional SBLIs. Figure 12 showed that this particular set of scaling parameters resulted in different trends in the data, and this variety in the trends was greater than the uncertainty associated with the measurement techniques. It is to be noted here that the data points with large values of of L^* and S_e^* correspond to the high Mach number ($M > 3$) experiments of Chapman *et al.* (1958), Pate (1964) and Threadgill *et al.* (2021), where large flow deflections could be imposed.

The reason why such a scaling worked for the compilation of turbulent SBLIs by Souverein

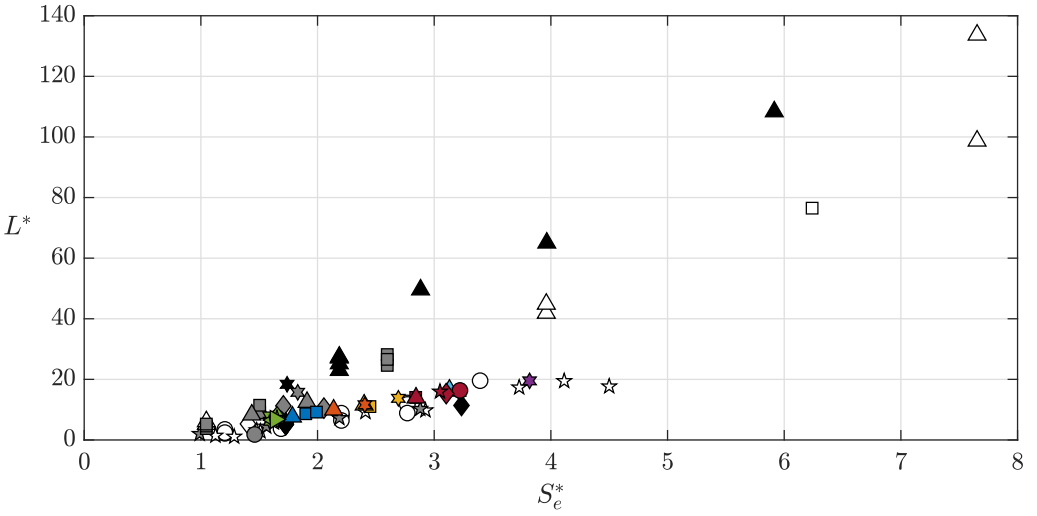

Figure 12: Length of interaction based on the mass-balance scaling by Souverein *et al.* (2013) with $k = 9$ (legend: refer to table 4).

Symbol	Literature	M	Re_i ($\times 10^6$)	φ	p_3/p_1
	Oblique Shock Reflections				
○	Barry *et al.* (1951)	2.1	0.11 - 1.20	3.0°- 7.0°	1.4 - 2.1
◊	Chapman *et al.* (1958)	2.4	0.18	4.0°	1.6
☆	Hakkinen *et al.* (1959)	2.0	0.30 - 0.44	2.7°- 8.4°	1.3 - 2.4
●	Degrez *et al.* (1987)	2.2	0.11	3.8°	1.5
⧫	Skebe *et al.* (1987)	2.0 - 3.0	0.52 - 0.62	4.5°- 5.5°	1.6 - 2.2
◆	Bur & Garnier (2016)	1.6	0.61 - 1.09	3.0°	1.3
★	Giepman *et al.* (2018)	1.7	1.8 - 2.5	2.0°- 5.0°	1.2 - 1.6
	Diop (2017)	1.7	0.62 - 1.24	3.0°- 6.0°	1.4 - 1.8
	Compression Ramps				
□	Chapman *et al.* (1958)	2.6	0.33	25°	4.3
△	Pate (1964)	3.0	0.28 - 0.77	25°	4.9
✶	Nielsen *et al.* (1965)	2.6	0.21	10°	1.9
■	Gray (1967)	3.0	0.19 - 1.03	7.5°- 15°	1.7 - 2.8
▲	Sfeir (1969)	2.7	0.14	9°- 11°	1.8 - 2.1
✶	Baroth & Holt (1983)	2.4	0.21	10°	1.8
▲	Threadgill *et al.* (2021)	4.0	0.11 - 0.25	15°- 28°	3.7 - 8.3
	Current Experiments	1.65	0.65 - 1.27	6°- 10°	1.3 - 1.6

Table 4: Legend of symbols for the compilation of transitional SBLIs (the legend for the experiments of Diop (2017) and the current experiments can be found in table 3).

et al. (2013), was because Reynolds number had a weak effect on the separation criterion of turbulent SBLIs. One of the possible reasons why this scaling did not collapse the data set of transitional SBLIs was due to the inability of the shock strength scaling to take into account the effect of Reynolds number. This was clear when looking at experiments where the Reynolds number was varied while keeping the shock strength constant (similar to the current experiments, see figure 11). Such data points fell on a straight vertical line with smaller lengths for higher Reynolds numbers (e.g. length scales reported by Threadgill *et al.* (2021)). Hence, this compilation highlighted that there was a need for the shock strength parameter to consider the change in Reynolds number.

In order to introduce Reynolds number in the shock strength scaling, the concept of free-interaction theory by Chapman *et al.* (1958) was revisited. The main idea behind this formulation was that the non-dimensional pressure rise at separation showed universal behaviour for all SBLIs (apart from the constant being different for turbulent and laminar SBLIs). This universal behaviour has been proven many times for a number of experiments for different Mach numbers, Reynolds numbers and shock strengths (Babinsky & Harvey 2011). Moreover, this universal behaviour was also verified for the current set of experiments as well (figure 8).

The initial idea of Souverein *et al.* (2013) for the non-dimensional shock strength scaling, was to compare the overall increase in pressure across the interaction with the pressure rise across separation $(\Delta p/(\Delta p)_{sep})$. Such a scaling did indeed collapse a subset of experimental data, in which the pressure rise needed to separate the boundary layer was explicitly reported (see pg. 519, figure 7, Souverein *et al.* (2013)). However, to include other experimental data which did not measure the pressure rise needed to separate, $(\Delta p)_{sep}$ was replaced by a constant (equation 3.5).

The current compilation showed that Reynolds number had a significant effect on the pressure rise at separation for laminar and transitional SBLIs, and this behaviour could be universally described by free-interaction theory (equation 3.2). If the pressure required to separate a boundary layer was approximated as the plateau pressure i.e. $(\Delta p)_{sep} \approx p_2 - p_1$, then free-interaction theory can be re-written as follows:

$$\frac{(\Delta p)_{sep}}{q} = F_p \sqrt{\frac{2\, c_f}{(M^2-1)^{1/2}}} \tag{3.7}$$

Where $F_p = 1.5$ was the value of the free-interaction coefficient at plateau for laminar SBLIs. As the extent of the plateau in laminar and transitional SBLIs was quite large, the uncertainty in the determination of this coefficient at plateau would be lower than determining the exact value needed to separate a laminar boundary layer (Giepman *et al.* 2018). Consequently, the expression $\Delta p/(\Delta p)_{sep}$ was elaborated using equation 3.7 as follows:

$$S_d^* = \frac{p_3 - p_1}{(\Delta p)_{sep}} = \frac{1}{F_p} \sqrt{\frac{(M^2-1)^{1/2}}{2\, c_f}} \frac{2}{\gamma M^2} \left(\frac{p_3}{p_1} - 1 \right) \tag{3.8}$$

This expression was similar to equation 3.5, with an additional term (similar to k) which introduced the effect of Reynolds number through the skin-friction coefficient (c_f). However, the skin-friction coefficient was not reported by most of the experiments in this compilation due to its measurement complexity. Hence, the theoretical skin-friction coefficient for a compressible Blasius boundary layer (at the mean location of separation) was used. This was done to remain consistent across all data sets. The compilation of the experimental data using the new shock strength scaling is shown in figure 13.

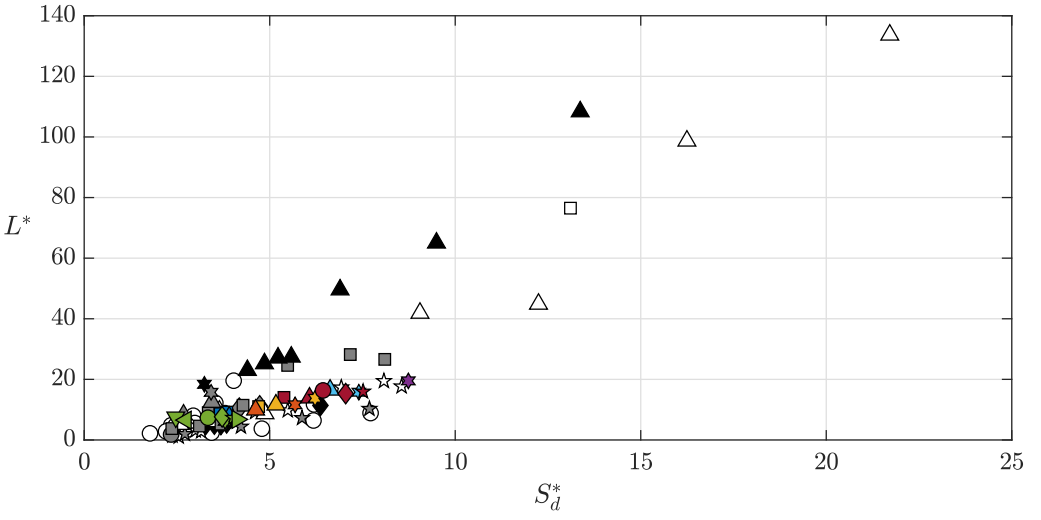

Figure 13: Compilation of length scales for a modified shock strength parameter, S_d^*.

This new scaling did improve some of the problems found in the previous scaling, in particular, different Reynolds number resulted in different separation criteria, and consequently the length scales did not fall on vertical lines (comparing figures 12 and 13). Nevertheless, there was still a large amount of scatter among the data, and hence proving that this was not the right scaling either.

Another way to scale the shock strength parameter was to compare the ratio of pressures, as opposed to comparing the pressure differences:

$$S_r^* = \frac{p_3/p_1}{(p/p_1)_{sep}} = \frac{p_3}{p_1}\left[1 + \frac{\gamma M^2}{2} F_p \sqrt{\frac{2\,c_f}{(M^2-1)^{1/2}}}\right]^{-1} \tag{3.9}$$

Where $(p/p_1)_{sep}$ is again obtained from the free-interaction theory of Chapman *et al.* (1958), by re-writing equation 3.7.

This latest scaling seemed to collapse most of the data set, as shown in figure 14. The effect of Reynolds number appeared to be well captured by this new scaling as the data points did not fall on a vertical line as the previous scaling (figure 12) and instead of the different trends observed in figure 13, the same linear relationship (i.e. same slope) was obtained for most of the data points from the compilation in figure 14.

The non-dimensional nature of this scaling automatically adjusted the shock strength; for low shock strengths with no separation, the imposed adverse pressure ratio is lower than the pressure ratio required to separate the boundary layer and hence, $S_r^* < 1$. For incipient interactions involving intermittent separation, the imposed pressure ratio is close to the pressure ratio required to separate the boundary layer ($S_r^* \approx 1$). And finally $S_r^* > 1$ corresponded to a typical separated SBLI. No empirical constant had to be adjusted for this auto-scaling, compared to equation 3.5.

Additionally, when the plateau pressure between separation and reattachment was represented as p_2, this separation criterion could be re-written as:

$$S_r^* = \frac{p_3/p_1}{(p/p_1)_{sep}} \approx \frac{p_3/p_1}{p_2/p_1} \approx \frac{p_3}{p_2} \tag{3.10}$$

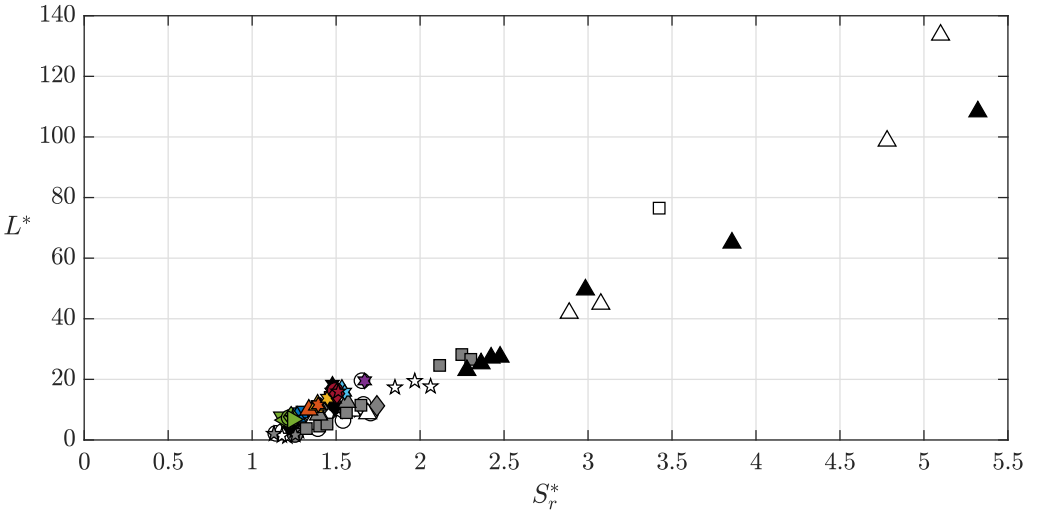

Figure 14: Compilation of length scales for different non-dimensional shock strengths, S_r^*.

It is well known that separated SBLIs are characterized by a two-step pressure rise over the interaction, and the overall pressure rise (p_3/p_1) across the interaction can be expressed as the combination of these two pressure jumps:

$$\frac{p_3}{p_1} = \frac{p_2}{p_1} \times \frac{p_3}{p_2} \tag{3.11}$$

The first pressure rise (p_2/p_1) at separation, exhibited universal behaviour according to free-interaction theory (Chapman *et al.* 1958). The second pressure rise (p_3/p_2) at reattachment, did not show universal behaviour. The collapse of the experimental data in figure 14 suggested that the non-dimensional length of interaction was only a function of the second pressure rise (p_3/p_2), given that the first pressure rise at separation was universal. This could be a possible physical explanation as to why only this separation criterion was able to collapse the experimental data set.

It is important to note that, as a consequence of this non-dimensional scaling, both the horizontal and vertical axes of figure 14 were functions of Reynolds numbers:

$$L^* \approx L\sqrt{\frac{Re_u}{x_s}}\, f(M,\varphi), \qquad S_r^* \approx (Re_u\, x_s)^{1/4}\, f(M,\varphi) \tag{3.12}$$

δ^* introduced a Reynolds number term through the Blasius reference length scale in L^*, while $(c_f)^{-1/2}$ introduced a Reynolds number term in S_r^*, where x_s was the mean location of separation of the boundary layer at the wall. Although it was of concern that the presence of a Reynolds number term on both axes of figure 14 might have contributed to the collapse, this contribution was found to be minimal, given that the exponent was not the same for the non-dimensional length and non-dimensional shock strength.

Looking closely at figure 14, it was observed that certain data sets from different wind tunnels exhibited the same slope, while being offset with respect to each other, along the vertical axis. Figure 15 shows the "zoom" of the data points in the lower left corner of figure 14, to highlight the low Mach number experiments (e.g. the current experiments). In fact, nearly parallel lines could be drawn, where each line corresponded to a subset from different wind tunnel facilities (parallel red lines in figure 15).

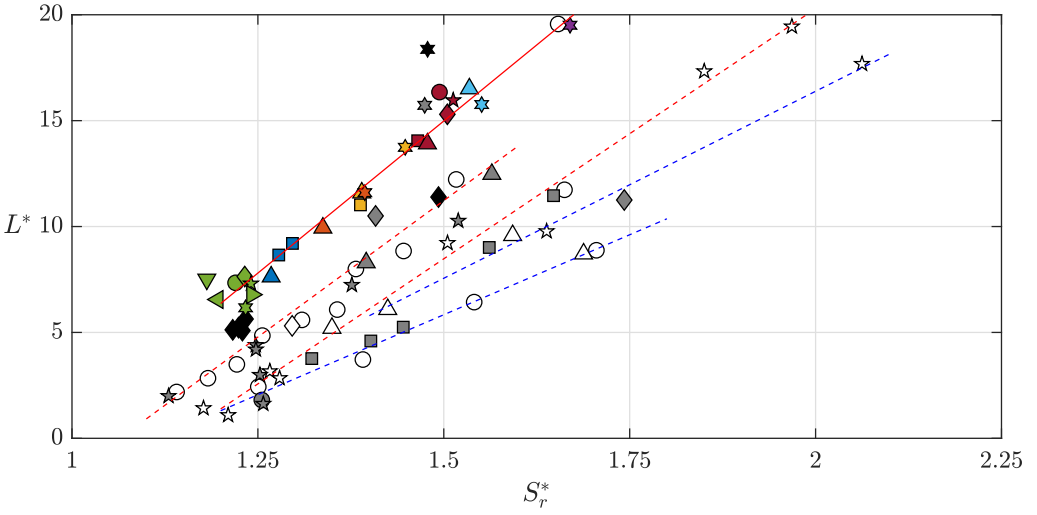

Figure 15: subset of the compilation from figure 14.

One of the major contributing factor for this nearly constant offset could be a difference in free-stream turbulence intensities across different wind tunnel facilities. The problem of background aerodynamic noise was found to be a major limitation in the study of high-speed laminar boundary layers since the very beginning of experiments in supersonic wind tunnels (Laufer 1954). Similar to low-speed flows, high free-stream turbulence intensities was linked to a rapid transition scenario that bypassed the linear growth of modes predicted by stability theory (Morkovin 1959).

Even if the free-stream turbulence intensities were low enough for the growth of linear and modal mechanisms (i.e. not high enough to trigger bypass transition) of the laminar boundary layer, it could still accelerate the natural transitional mechanisms (Laufer 1961). Consequently this acceleration could have enabled the separated boundary layer to reattach "earlier", leading to a shorter length of interaction, and subsequently an offset in figure 15. The influence of free-stream turbulence intensity on the transitional mechanisms of a laminar boundary layer is a complex topic, particularly, the effect of amplitude and spectral content of the free-stream noise on the transition process (through receptivity), is not very well understood. Not all wind tunnel facilities in this compilation have reported their amplitude and spectral content of the free-stream noise, and hence it was difficult to conclusively determine if and how these parameters affected the length scales of the interaction.

Nevertheless, a qualitative understanding of this effect of freestream noise is well known. A review of supersonic wind tunnels by Pate & Schueler (1969) provided strong evidence linking the noise radiated by turbulent boundary layers on the tunnel walls to lower transition Reynolds numbers. This prompted NASA to develop the so-called "quiet" wind tunnel, which ensured the boundary layers on all the tunnel walls to be laminar. Experiments performed in this low-disturbance tunnel reported transition Reynolds numbers of $\mathcal{O}(10^7)$, one order of magnitude higher than conventional "noisy" wind tunnels (Chen *et al.* 1989; Schneider 2004).

Schneider (2015) further highlighted that quiet tunnels were more representative of actual flight conditions, and emphasized the necessity to develop quiet wind tunnels to study the transition process, particularly at hypersonic speeds, where the boundary layer transitional mechanisms were more complex. Unfortunately, none of the experiments in this compilation

were made in quiet wind tunnels. It would be very interesting to compare the length scales for laminar and transitional SBLIs from such facilities to the current compilation.

Another important factor to consider was leading edge bluntness. Potter & Whitfield (1962) showed that the bluntness of the leading edge had a significant effect on the transition process of the laminar boundary layer. It was found that the transition Reynolds number increased for increasing "bluntness" of the leading edge, even when bluntness had a negligible effect on the mean pressure distribution. Given that the degree of bluntness of the leading edge was not reported by many of the authors in this compilation of experimental data, it was difficult to determine what kind of effect this had on the transition process of their respective boundary layers. This delay or acceleration of the transition process (corresponding to a blunt or sharp leading edge respectively) of the boundary layer could have affected the length scales of interaction, and consequently played a role in the observed offset in length scales in this compilation.

Moreover, Lusher & Sandham (2020) showed that the lateral walls of the wind tunnel test section could dramatically change the length of interaction for transitional SBLIs. This confinement effect was particularly significant when the span-wise width of the test section was small compared to the length of the separated region. The current compilation in figure 15 contained experiments with a wide variety of test section sizes. The effect of this finite size of the test section and deviation from nominally 2D interaction is a complicated relationship between the laminar boundary layer and the turbulent boundary layer on the side walls. This topic of 3D effects in nominally 2D SBLIs has received relatively more attention for turbulent interactions, with investigations from Dussauge *et al.* (2006); Burton & Babinsky (2012); Wang *et al.* (2015); Xiang & Babinsky (2019) to cite a few.

Moreover, Threadgill *et al.* (2021) showed that when the geometry did not span the entire width of the test section, "spillage" of the flow in the span-wise direction reduced the length of interaction, compared to when end-plates were used. This could have played a contributing factor on the smaller length scales reported by the experiments of Degrez *et al.* (1987), where the flat plate did not span the entire width of the test section. However, it is important to note that such effects can both increase or decrease the length scales of the interaction, depending on the secondary flow conditions underneath the main geometry. In fact, an overpressure underneath the geometry could restrict spillage and increase the length of interaction as well.

Another contributing factor could be a systematic error introduced in the calculation of the length of interaction by different studies.

Additionally, figure 15 showed that some data points exhibited a different slope (shown in solid blue lines) compared to the rest of the compilation (shown in solid red lines).

The slope of this deviant subset of data was found to be reduced by 47% (when compared to the slope of red lines in figure 15). To understand this deviation, comparisons were made with individual experimental data sets in figure 16.

The current experiments were compared with one of the first parametric studies on transitional SBLIs from Barry *et al.* (1951) in figure 16a. It was observed that at low Reynolds numbers (i.e. $Re_i = 0.11 \times 10^6$), the same slope was observed (compared to the current experiments), albeit with an offset (possibly due to a combination of factors mentioned before). However, as Reynolds number was increased (i.e. $Re_i \geq 0.6 \times 10^6$), this slope reduced and the offset also increased (the change in offset is more clear at higher $S_r^\star$). It is important to note here that Reynolds number was changed by changing the total pressure of the free-stream, while the inviscid shock impingement location was kept constant.

Similarly, comparisons were made with the more recent parametric studies of Giepman *et al.* (2018) in figure 16b. At "low" Reynolds numbers (i.e. $Re_i = 1.8 \times 10^6$), when the imposed flow deflection was increased, the measured length scales were offset with respect to the current experiments and the slope was slightly lower. However, as the Reynolds number

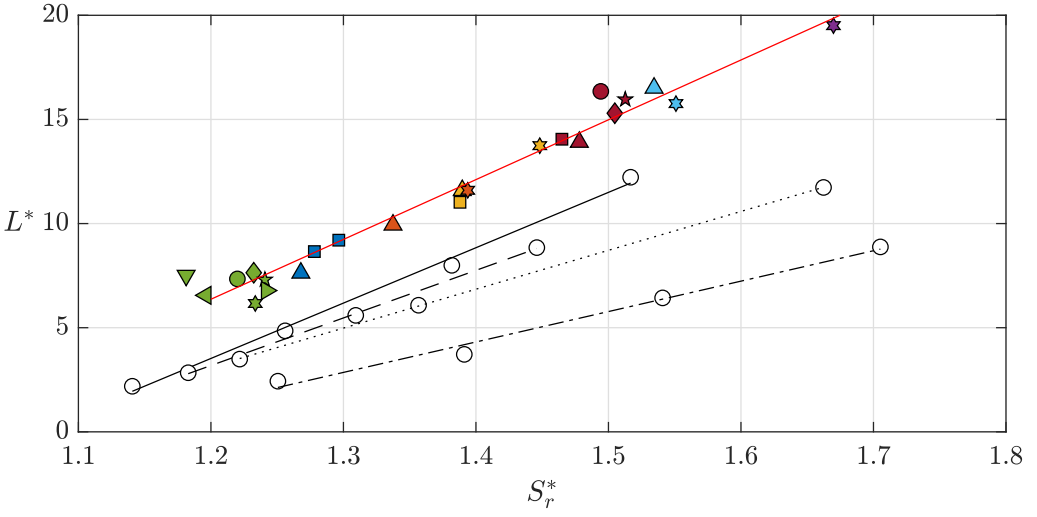

(a) Comparison with the experiments of Barry *et al.* (1951) (symbol ○) different Reynolds numbers (solid black line: $Re_i = 0.11 \times 10^6$, dashed black line: $Re_i = 0.25 \times 10^6$, dotted black line $Re_i = 0.6 \times 10^6$, dashed dotted black line $Re_i = 1.2 \times 10^6$).

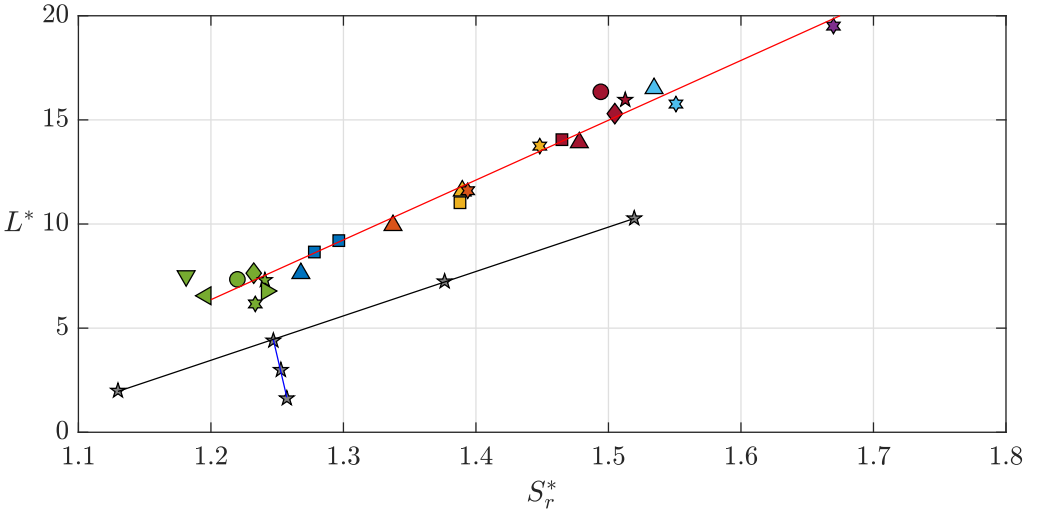

(b) Comparison with the experiments of Giepman *et al.* (2018) (symbol★) for a constant Reynolds number (solid black line: $Re_i = 1.8 \times 10^6, 2° \leq \varphi \leq 5°$) and increasing Reynolds number (solid blue line: $\varphi = 3°, 1.8 \leq Re_i\ (\times 10^6) \leq 2.5$).

Figure 16: Reynolds number effect (legend of symbols: refer to table 4).

was increased (i.e. $Re_i > 1.8 \times 10^6$, corresponding to the solid blue line in figure 16b), the offset increased as well (in this case the Reynolds number was increased by moving the shock impingement location further downstream, while keeping the same total pressure of the freestream).

Moreover, it is also imperative to note that there was an order of magnitude difference in Reynolds numbers between the experiments of Barry *et al.* (1951) and Giepman *et al.* (2018). Hence, the lowest Reynolds number of Giepman *et al.* (2018) was still higher than the highest Reynolds number of Barry *et al.* (1951), while the offset for both of these experiments were

nearly the same, possibly suggesting that the free-stream noise of Giepman *et al.* (2018) was much lower than that of Barry *et al.* (1951).

In essence, figure 16 conveyed that while the new separation criterion (S_r^*) was able to capture the effects of Reynolds number, it was merely a first order effect that worked when the free-stream noise of the wind tunnel was relatively low (e.g. the current experiments). For higher free-stream noise, the transitional mechanisms of the laminar boundary layer were possibly accelerated, which could have changed the relationship between Reynolds number and the length of interaction. The modelling of this modified relationship would require insight into the complex interplay between freestream noise, receptivity (both for the attached and separated boundary layer) and Reynolds number. Hence, this observed offset in these curves as well as the change in slope, could have multiple contributing factors, which requires additional experiments and analyses to understand in more detail.

3.4. *Universal scaling*

Notwithstanding the non-linear effects of the transition process, it seemed that the new separation criterion scaling S_r^* was able to capture the relationship between the length of interaction and the imposed adverse pressure gradient, for laminar and transitional SBLIs. Building on these results, an attempt was made to extend this scaling for turbulent SBLIs as well.

For turbulent SBLIs, a compilation of experimental data sets was already made by Souverein *et al.* (2013) (figure 1). And, it was shown that the pressure required to separate a turbulent boundary layer was only a function of the dynamic pressure of the free-stream (see figure 8 from Souverein *et al.* (2013)). This meant that Reynolds number had a weak influence on the pressure required to separate a turbulent boundary layer. Subsequently, this pressure ratio required to separate turbulent boundary layers was determined as follows:

$$\frac{(\Delta p)_{sep}}{q} \approx \mathcal{K} \tag{3.13a}$$

$$\left(\frac{p}{p_1}\right)_{sep} \approx 1 + \frac{\gamma M^2}{2}\mathcal{K} \tag{3.13b}$$

Where the constant $\mathcal{K} \approx 0.4$ was found by Souverein *et al.* (2013). It was observed that the constant $\mathcal{K}$ replaced the term with the skin-friction coefficient, when compared with equation 3.7, and thus removing the effect of Reynolds number.

Consequently, the shock strength scaling proposed here could also be applied to turbulent SBLIs, albeit with a modified resulting expression, when compared with laminar and transitional SBLIs (equation 3.9).

$$S_r^* = \frac{p_3/p_1}{(p/p_1)_{sep}} = \frac{p_3}{p_1}\left[1 + \frac{\gamma M^2}{2}\mathcal{K}\right]^{-1} \tag{3.14}$$

The compilation made by Souverein *et al.* (2013) was revisited using this new scaling and is shown in figure 17. It was found that this new shock strength scaling did indeed work also for turbulent SBLIs. As opposed to the best fit (based on a power law) proposed by Souverein *et al.* (2013), a first order (linear) polynomial fit was made in the current analysis, where two different slopes was identified depending on whether the interaction was attached ($S_r^* < 1$) or separated ($S_r^* > 1$).

The slope was more than four times higher when a mean separation was found when compared to an incipient separation (table 5). Additionally, the scatter in the length scales

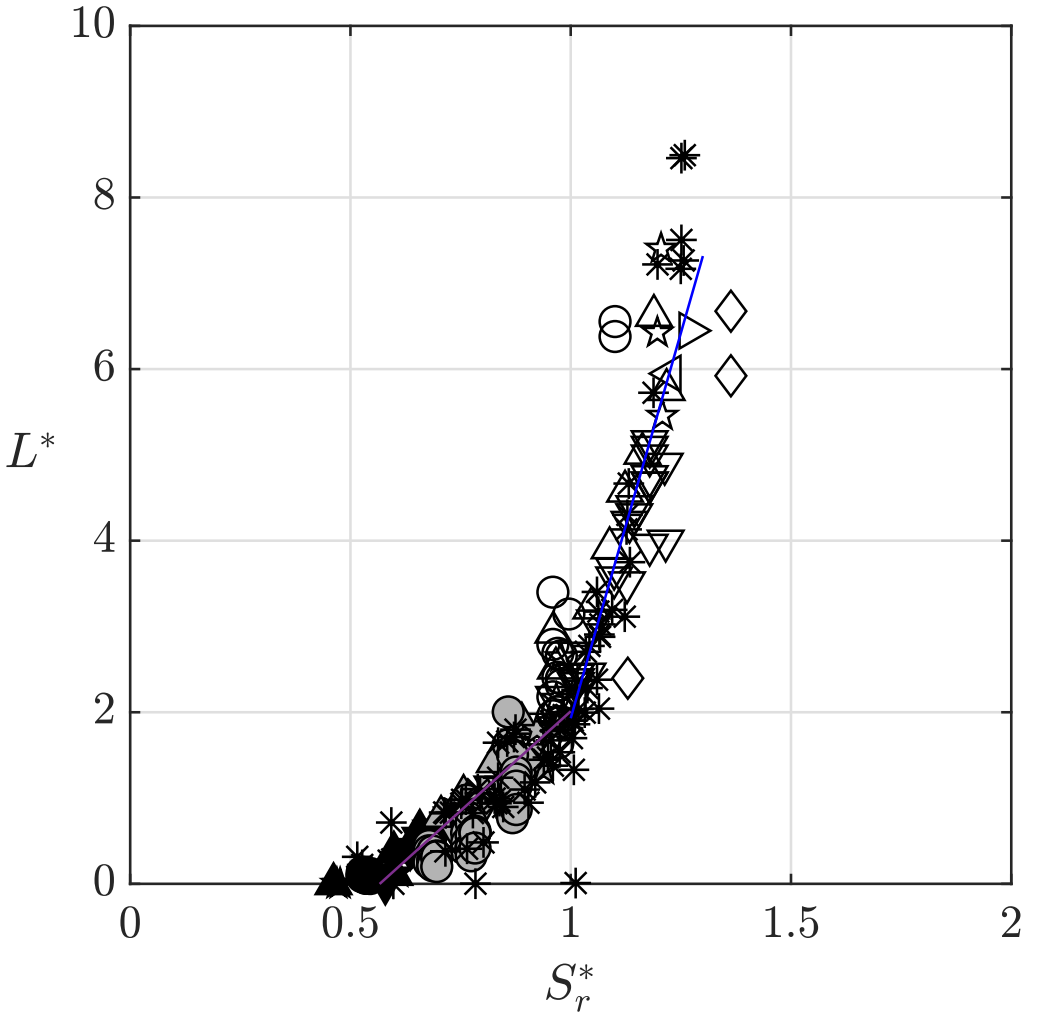

Figure 17: Evolution of length scales for turbulent SBLIs using the new scaling (legend: refer to Souverein *et al.* (2013)).

increased for very high (relatively speaking) shock strengths i.e. $S_r^* > 1.2$, where large imposed flow deflections might have resulted in significant corner and/or 3D effects. Moreover, large flow deflections probably resulted in a Mach stem over the turbulent SBLI, which could have saturated the imposed pressure jump across the interaction. Hence, higher non-dimensional shock strengths might not have been possible in the supersonic regime of turbulent SBLIs. Hence, the confidence of this slope at higher separation criteria was low. It is important to note that SBLI studies made in the hypersonic regime were not included in this compilation as wall heat transfer effects become significant. Jaunet *et al.* (2014) had shown that non-adiabatic wall conditions also affected the separation criterion at supersonic speeds. In such cases, the separation criterion would have to be further modified to take this into account, which was not performed in the current analysis.

Due to the universality of this scaling of the separation crtierion, laminar, transitional and turbulent SBLIs can now be compared directly and figure 18 shows this comparison. The black and white symbols correspond to turbulent SBLI experiments (taken from Souverein *et al.*

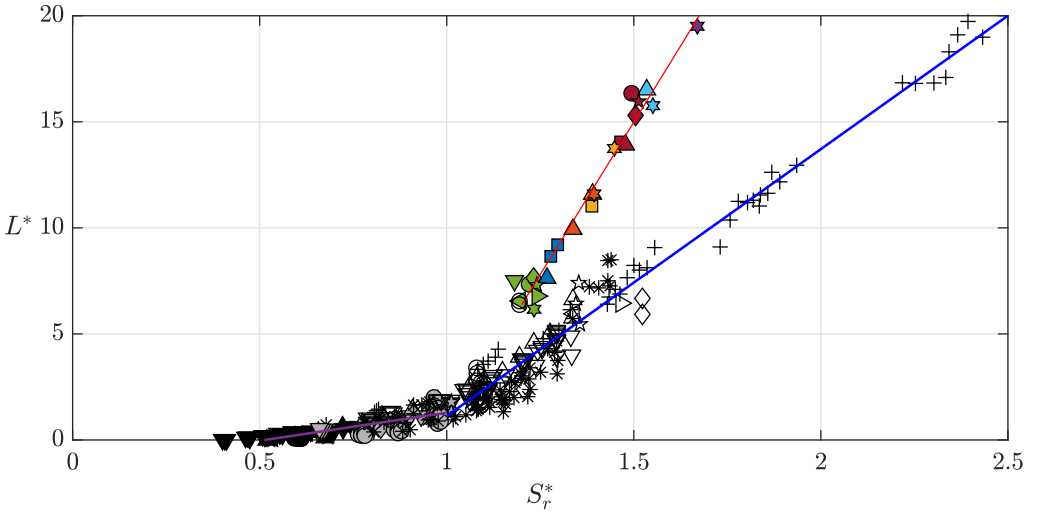

Figure 18: Comparison of turbulent and laminar SBLI length scales (legend: refer to Souverein *et al.* (2013) for black and white symbols, and refer to table 3 for coloured symbols).

	Laminar & Transitional SBLIs	Turbulent SBLIs
$S_r^* < 1$		(4.6,-2.6)
$S_r^* > 1$	(28.7,-28.1)	(18.0,-16.0)
Deviated subset	(15.1,-16.8)	

Table 5: Coefficients (a,b) of first order polynomial fit: $L^* = a\, S_r^* + b$.

(2013)) and the coloured symbols correspond to the current experiments on transitional SBLIs (refer to table 3). To the authors' knowledge, this is the first time such a direct comparison has been made between the different types of SBLIs. To avoid clutter and improve legibility, only the current experiments from the compilation of laminar and transitional SBLIs are shown in figure 18.

It was observed that there was little overlap between the two compilations. This was mostly due to the fact that the pressure ratio required to separate a laminar boundary layer is much lower compared to a turbulent boundary layer, resulting in large separation criteria for laminar and transitional SBLIs. Consequently, the non-dimensional lengths scales of laminar and transitional SBLIs were also much larger relative to turbulent SBLIs.

Given this small overlap between the length scales, it was difficult to conclusively conclude on the difference in slope between the different types of SBLIs. The power law fit of Souverein *et al.* (2013) suggested an asymptotic increase of length scales of turbulent SBLIs for $S_r^* > 1.2$, however, there wasn't enough data points in this regime to support this behaviour conclusively. As mentioned before, experiments of turbulent SBLIs at $S_r^* > 1.2$ were possibly characterized by significant corner and/or 3D effects, which would have affected the observed length scales.

Nevertheless, a linear fit of these experimental data sets showed that the slope of laminar and transitional SBLIs were approximately 60% larger than the slope of turbulent SBLIs (table 5). In fact, the subset of laminar and transitional SBLIs that deviated away from the

rest of the compilation exhibited similar slopes as that of turbulent SBLIs. Again suggesting that this subset of laminar and transitional SBLIs possibly involved a laminar boundary layer that was strongly affected by its transition process, and likely a non-canonical SBLI. The slopes of all the types of SBLIs are shown in table 5 for reference.

Figure 18 also suggested a possible continuity in the non-dimensional lengths between turbulent and laminar SBLIs. To elaborate, this would mean that if experiments of laminar and transitional SBLIs were made at the separation criteria corresponding to turbulent SBLIs (i.e. $S_r^* < 1.2$), then the resulting non-dimensional lengths of interaction could possibly be similar (or in the same range of values) to turbulent SBLIs. This suggested that the L^* scaling was able to reconcile large differences (nearly one order of magnitude) in the aspect ratios of the length scales (L/δ^*) between the different types of SBLIs, through the inviscid term in equation 3.4:

$$\left.\begin{aligned}(L/\delta^*)_{laminar} &> (L/\delta^*)_{turbulent}\\ (G_3)_{laminar} &< (G_3)_{turbulent}\end{aligned}\right\} (L^*)_{laminar} \approx (L^*)_{turbulent} \tag{3.15}$$

This suggested that this set of non-dimensional scaling (L^* and S_r^*) were universal for the types of SBLIs considered in this compilation.

4. Conclusion

Experiments of transitional SBLI were made on nominally 2D compression ramps. Two ramp geometries, with a 6° and 10° flow deflection were studied at a Mach number of 1.65 and the unit Reynolds number was varied between 5.6 million per metre and 11 million per metre. The canonical nature of the transitional SBLI was verified with comparisons with free-interaction theory.

The non-dimensional scaling of the length of interaction (originally proposed by Souverein *et al.* (2013)), based on the mass-balance between the incoming and outgoing boundary layer was found to reconcile the differences in absolute length scales between compression ramp SBLIs and transitional oblique shock reflection experiments of Diop (2017). Thus, such a mass-balance scaling also worked for laminar and transitional SBLIs.

A compilation of lengths of interaction reported from various experiments on transitional SBLIs in literature was made for the first time. The compilation showed that different trends were observed by subsets, and highlighted the effects of Reynolds number on the separation criteria.

A new non-dimensional scaling was developed for the shock strength that included the effects of Reynolds number through the free-interaction theory. In particular, this new scaling was based on the ratio of pressures across the interaction as opposed to the difference in pressures across the interaction (as originally proposed by Souverein *et al.* (2013)). The pressure ratio across the interaction was normalized with the pressure ratio required to separate the boundary layer, which was obtained from free-interaction theory. Such a scaling was able to collapse most of the data set, and nearly the same linear relationship between this new separation criterion and the length of interaction was obtained for all the data points.

The current experiments on transitional SBLIs (performed in the IUSTI laboratory) were found to have the longest non-dimensional lengths of interaction compared to the rest of the compilation. And, it was observed that some subsets exhibited an offset in non-dimensional length scales with respect to the current experiments. Many possible factors were identified that could have contributed to this offset, including higher free-stream noise, leading edge bluntness, and 3D effects. However, a conclusive cause for this offset could not be found. Additionally, other subsets showed different slopes entirely, compared to the rest of the

compilation. While a conclusive cause could not be identified, the most likely cause was found to be the combination of high free-stream noise and high Reynolds number, resulting in a non-canonical laminar boundary layer and SBLI.

The scaling of the separation criterion based on the ratio of pressures across the interaction was extended to turbulent SBLIs. Contrary to laminar and transitional SBLIs, Souverein *et al.* (2013) had shown that Reynolds number had a weak effect on the pressure required to separate a turbulent boundary layer. Hence, this weak effect of Reynolds number was incorporated into the new separation criterion through an empirical constant. This new scaling of separation criterion was indeed able to collapse most of the data set from the compilation of Souverein *et al.* (2013).

Due to the common non-dimensional formulation of the length scales and separation criteria between laminar, transitional and turbulent SBLIs, a direct comparison was made between the different types of SBLIs for the first time. Although there was little overlap, the comparison suggested that the non-dimensional lengths of interaction between different types of SBLIs were similar for equivalent separation criteria. To elaborate, although large differences can be found when comparing the aspect ratio (L/δ^*) between different SBLIs, the length of interaction represented in terms of L^* were similar.

Further experiments and analyses are required to confirm and validate this hypothesis for different separation criteria, as well as reaffirm the growth rates of the length scales across different types of SBLIs for increasing separation criteria.

Acknowledgements. The authors would like to acknowledge the technical support of Pierre Lantoine while performing the experiments in the wind tunnel.

Funding. This work is part of the European TEAMAero project (Towards Effective Flow Control and Mitigation of Shock Effects in Aeronautical Applications). The authors would like to acknowledge the support from the European Union's Horizon 2020 research and innovation programme under grant agreement No. EC grant 860909.

Declaration of interests. The authors report no conflict of interest.

Author ORCID. Nikhil Mahalingesh, https://orcid.org/0000-0002-5677-1897; Sébastien Piponniau, https://orcid.org/0000-0002-4918-0669, Pierre Dupont, https://orcid.org/0000-0002-5495-303X

Author contributions. The experiments were performed by all three authors. The data analysis and writing was performed by Nikhil Mahalingesh. The editing and corrections were performed by Sébastien Piponniau and Pierre Dupont.

REFERENCES

Babinsky, Holger & Harvey, John K 2011 *Shock wave-boundary-layer interactions*, , vol. 32. Cambridge University Press.

Baroth, Edmund Craig & Holt, M 1983 Investigation of supersonic separated flow in a compression corner by laser doppler anemometry. *Experiments in fluids* **1** (4), 195–203.

Barry, Frank William, Shapiro, Ascher H & Neumann, Ernest Paul 1951 The interaction of shock waves with boundary layers on a flat surface. *Journal of the Aeronautical Sciences* **18** (4), 229–238.

Bur, Reynald & Garnier, Eric 2016 Transition effect on a shock-wave/boundary layer interaction. In *The CAero2 Platform: Dissemination of Computational Case Studies in Aeronautics, ECCOMAS Congress*, pp. 5–10.

Burton, DMF & Babinsky, Holger 2012 Corner separation effects for normal shock wave/turbulent boundary layer interactions in rectangular channels. *Journal of Fluid Mechanics* **707**, 287–306.

Chapman, Dean R, Kuehn, Donald M & Larson, Howard K 1958 Investigation of separated flows in supersonic and subsonic streams with emphasis on the effect of transition. *Tech. Rep.*. Ames Aeronautical Laboratory.

712 Chen, F-J, Malik, MR & Beckwith, IE 1989 Boundary-layer transition on a cone and flat plate at mach
713 3.5. *AIAA journal* **27** (6), 687–693.
714 Degrez, Gérard, Boccadoro, CH & Wendt, John F 1987 The interaction of an oblique shock wave with
715 a laminar boundary layer revisited. an experimental and numerical study. *Journal of fluid mechanics*
716 **177**, 247–263.
717 Délery, Jean, Marvin, John G & Reshotko, Eli 1986 Shock-wave boundary layer interactions. *Tech.*
718 *Rep.*. Advisory Group for Aerospace Research and Development Neuilly-Sur-Seine (France).
719 Diop, Moussa 2017 Transition à la turbulence en écoulements compressibles décollés. PhD thesis, Aix-
720 Marseille.
721 Diop, Moussa, Piponniau, Sébastien & Dupont, Pierre 2016 On the length and time scales of a laminar
722 shock wave boundary layer interaction. In *54th AIAA Aerospace Sciences Meeting*, p. 0073.
723 Diop, Moussa, Piponniau, Sébastien & Dupont, Pierre 2019 High resolution lda measurements in
724 transitional oblique shock wave boundary layer interaction. *Experiments in Fluids* **60** (4), 1–15.
725 Dolling, David S 2001 Fifty years of shock-wave/boundary-layer interaction research: what next? *AIAA*
726 *journal* **39** (8), 1517–1531.
727 Dupont, Pierre, Haddad, C & Debieve, JF 2006 Space and time organization in a shock-induced separated
728 boundary layer. *Journal of fluid Mechanics* **559**, 255–277.
729 Dussauge, Jean-Paul, Dupont, Pierre & Debiève, Jean-Francois 2006 Unsteadiness in shock wave
730 boundary layer interactions with separation. *Aerospace science and Technology* **10** (2), 85–91.
731 Gadd, GE 1958 Interactions between shock waves and boundary layers. In *Grenzschichtforschung/Boundary*
732 *Layer Research: Symposium Freiburg/Br. 26. Bis 29. August 1957/Symposium Freiburg/Br. August*
733 *26–29, 1957*, pp. 239–255. Springer.
734 Gadd, GE, Holder, Douglas William & Regan, JD 1954 An experimental investigation of the interaction
735 between shock waves and boundary layers. *Proceedings of the Royal Society of London. Series A.*
736 *Mathematical and Physical Sciences* **226** (1165), 227–253.
737 Giepman, RHM, Schrijer, FFJ & Van Oudheusden, BW 2018 A parametric study of laminar and
738 transitional oblique shock wave reflections. *Journal of Fluid Mechanics* **844**, 187–215.
739 Gray, J Don 1967 *Investigation of the effect of flare and ramp angle on the upstream influence of laminar*
740 *and transitional reattaching flows from Mach 3 to 7*. Arnold Engineering Development Center, Von
741 Kármán Gas Dynamics Facility, Air . . . .
742 Hakkinen, Raimo Jaakko, Greber, Isaac, Trilling, Leon & Abarbanel, SS 1959 The interaction of an
743 oblique shock wave with a laminar boundary layer. *Tech. Rep.*.
744 Jaunet, V, Debieve, JF & Dupont, P 2014 Length scales and time scales of a heated shock-wave/boundary-
745 layer interaction. *AIAA Journal* **52** (11), 2524–2532.
746 Larchevêque, Lionel 2016 Low-and medium-frequency unsteadinesses in a transitional shock–boundary
747 reflection with separation. In *54th AIAA aerospace sciences meeting*, p. 1833.
748 Laufer, John 1954 Factors affecting transition reynolds numbers on models in supersonic wind tunnels.
749 *Journal of the Aeronautical Sciences* **21** (7), 497–498.
750 Laufer, John 1961 Aerodynamic noise in supersonic wind tunnels. *Journal of the Aerospace Sciences*
751 **28** (9), 685–692.
752 Lees, Lester 1949 *Interaction between the laminar boundary layer over a plane surface and an incident*
753 *oblique shock wave*. Princeton University, Aeronautical Engineering Laboratory.
754 Lewis, John E, Kubota, Toshi & Lees, Lester 1968 Experimental investigation of supersonic laminar,
755 two-dimensional boundary-layer separation in a compression corner with and without cooling. *AIAA*
756 *journal* **6** (1), 7–14.
757 Liepmann, Hans Wolfgang, Roshko, Anatol & Dhawan, Satish 1952 On reflection of shock waves
758 from boundary layers. *Tech. Rep.*.
759 Lusher, David J & Sandham, Neil D 2020 The effect of flow confinement on laminar shock-wave/boundary-
760 layer interactions. *Journal of Fluid Mechanics* **897**, A18.
761 Mack, LM 1954 An experimental investigation of the temperature recovery factor. *Jet Propulsion Lab.*
762 *Report* pp. 20–80.
763 Marxen, Olaf & Henningson, Dan S 2011 The effect of small-amplitude convective disturbances on the
764 size and bursting of a laminar separation bubble. *Journal of Fluid Mechanics* **671**, 1–33.
765 Morkovin, Mark V 1959 On supersonic wind tunnels with low free-stream disturbances .
766 Nielsen, Jack N, Lynes, Larry L & Goodwin, Frederick K 1965 Calculation of laminar separation with
767 free interaction by the method of integral relations, part i-two-dimensional supersonic adiabatic flow.
768 In *Vidya Report No. 185, AFFDL-TR-65-107*. Wright-Patterson AFB Ohio.

769 Oswatitsch, Klaus & Wieghardt, K 1948 *Theoretical analysis of stationary potential flows and boundary*
770 *layers at high speed*. National Advisory Commitee for Aeronautics.
771 Pate, SR 1964 Investigation of flow separation on a two-dimensional flat plate having a variable-span
772 trailing-edge flap at m infinity equal to 3 and 5. *(No Title)* .
773 Pate, Samuel R & Schueler, CJ 1969 Radiated aerodynamic noise effects on boundary-layer transition in
774 supersonic and hypersonic wind tunnels. *AIAA Journal* **7** (3), 450–457.
775 Polivanov, Pavel A, Sidorenko, Andrey & Maslov, Anatoly 2015 Transition effect on shock
776 wave/boundary layer interaction at m= 1.47. In *53rd AIAA Aerospace Sciences Meeting*, p. 1974.
777 Potter, J Leith & Whitfield, Jack D 1962 Effects of slight nose bluntness and roughness on boundary-layer
778 transition in supersonic flows. *Journal of Fluid Mechanics* **12** (4), 501–535.
779 Roberts, Melvin L 1970 Transitional flow separation upstream of a compression corner. *Journal of*
780 *Spacecraft and Rockets* **7** (9), 1113–1117.
781 Schneider, Steven P 2004 Hypersonic laminar–turbulent transition on circular cones and scramjet
782 forebodies. *Progress in Aerospace Sciences* **40** (1-2), 1–50.
783 Schneider, Steven P 2015 Developing mechanism-based methods for estimating hypersonic boundary-
784 layer transition in flight: The role of quiet tunnels. *Progress in Aerospace Sciences* **72**, 17–29.
785 Sfeir, Abdallah Antoun 1969 *Supersonic laminar boundary layer separation near a compression corner*.
786 University of California, Berkeley.
787 Skebe, Stanley A, Greber, Isaac & Hingst, Warren R 1987 Investigation of two-dimensional shock-
788 wave/boundary-layer interactions. *AIAA journal* **25** (6), 777–783.
789 Souverein, LJ, Bakker, PG & Dupont, P 2013 A scaling analysis for turbulent shock-wave/boundary-layer
790 interactions. *Journal of Fluid Mechanics* **714**, 505–535.
791 Threadgill, James AS, Little, Jesse C & Wernz, Stefan H 2021 Transitional shock boundary layer
792 interactions on a compression ramp at mach 4. *AIAA journal* **59** (12), 4824–4841.
793 Wang, Bo, Sandham, Neil D, Hu, Zhiwei & Liu, Weidong 2015 Numerical study of oblique shock-
794 wave/boundary-layer interaction considering sidewall effects. *Journal of Fluid Mechanics* **767**, 526–
795 561.
796 Xiang, Xue & Babinsky, Holger 2019 Corner effects for oblique shock wave/turbulent boundary layer
797 interactions in rectangular channels. *Journal of Fluid Mechanics* **862**, 1060–1083.